Experimental Mechanics
DOI 10.1007/s11340-017-0335-6

Evaluation of the Effect of Thermal Oxidation and Moisture on the Interfacial Shear Strength of Unidirectional IM7/BMI Composite by Fiber Push-in Nanoindentation

T. Xu[1] · H. Luo[1] · Z. Xu[1] · Z. Hu[1] · M. Minary-Jolandan[1] · S. Roy[2] · H. Lu[1]

Received: 22 January 2017 / Accepted: 21 August 2017

Abstract Fiber push-in nanoindentation is conducted on a unidirectional carbon fiber reinforced bismaleimide resin composite (IM7/BMI) after thermal oxidation to determine the interfacial shear strength. A unidirectional IM7/BMI laminated plate is isothermally oxidized under various conditions: in air for 2 months at 195 °C and 245 °C, and immersed in water for 2 years at room temperature to reach a moisture-saturated state. The water-immersed specimens are subsequently placed in a preheated environment at 260 °C to receive sudden heating, or are gradually heated at a rate of approximately 6 °C/min. A flat punch tip of 3 μm in diameter is used to push the fiber into the matrix while the resulting load-displacement data is recorded. From the load-displacement data, the interfacial shear strength is determined using a shear-lag model, which is verified by finite element method simulations. It is found that thermal oxidation at 245 °C in air leads to a significant reduction in interfacial shear strength of the IM7/BMI unidirectional composite, while thermal oxidation at 195 °C and moisture concentration have a negligible effect on the interfacial shear strength. For moisture-saturated specimens under a slow heating rate, there is no detectable reduction in the interfacial shear strength. In contrast, the moisture-saturated specimens under sudden heating show a significant reduction in interfacial shear strength. Scanning electron micrographs of IM7/BMI composite reveal that both thermal oxidation at 245 °C in air and sudden heating induced microcracks and debonding along the fiber/matrix interface, thereby weakening the interface, which is the origin of failure mechanism.

Keywords Carbon fibers · Polymer-matrix composites · Interfacial strength · Environmental degradation · Cohesive shear traction separation law · Finite element analysis

Introduction

Bismaleimide (BMI) composites have been used extensively for structural components in aircraft, including composite frames for turbine engines and engine exhaust washed structures due to a unique combination of high service temperature, reasonably high fracture toughness, and epoxy-like processing conditions [1, 2]. BMI composites, however, are known to have very limited service life under strenuous operational conditions due to chemical, physical, and mechanical degradation under harsh environmental conditions, such as temperature cycles and atmospheric humidity experienced in flight [3–5] and also in storage. Failure of composites in these aggressive environments has a direct impact on operational cost and fleet readiness. For an IM7/BMI unidirectional composite after exposure to 195 °C and 245 °C for 2 months, we have reported its dynamic compressive behavior at high strain rates [5]. The results obtained are used to show that thermal oxidation leads to a significant reduction in stiffness and strength. In a follow-up work [6], the dynamic compressive experiments are conducted to determine the effect of thermal oxidation on the mechanical properties of the BMI resin at high strain rates. The resin exposed to 245 °C for 1500 h shows only slightly reduced mechanical properties, which is in stark contrast to the data reported for IM7/BMI unidirectional composite oxidized for two months at 245 °C [5]. It indicates that

✉ H. Lu
hongbing.lu@utdallas.edu

[1] Department of Mechanical Engineering, The University of Texas at Dallas, Richardson, TX 75080, USA

[2] Department of Aerospace Engineering and Mechanics, University of Alabama, Tuscaloosa, AL 35487, USA

Published online: 31 August 2017

degradation in composites is likely due to matrix shrinkage and debonding at the interface between fibers and matrix. Consequently, measuring the thermal degradation of the neat resin is a necessary but not sufficient step for understanding the appropriate mechanism for synergistic degradation at the fiber/matrix interface in a composite. In this paper, an investigation is made to determine the effect of thermal oxidation on the fiber/matrix interface behavior directly using fiber push-in nanoindentation.

Composites absorb moisture not only during the flight but also in storage. Although it has been known that moisture-induced swelling may degrade the fiber/matrix interface [4], most of the literature investigating the moisture effect in polymer composites has placed an emphasis for predicting the diffusion of moisture. Much less attention is given to the degradation of fiber/matrix interface due to the long-term moisture effects [7, 8]. During normal operation, the moisture-saturated polymer composites can be subjected to rapid heating. If the heating is too fast for the absorbed moisture to escape, large internal water vapor pressures can develop and can lead to void nucleation in the matrix and at the fiber/matrix interface. This steam-induced delamination and blistering (referred as steam blistering effect) can potentially cause failure of the composite. This phenomenon has led to research interests from both experimental [9, 10] and theoretical perspectives [11, 12]. Most of the existing work, however, has been focused on understanding the effect of steam blistering on overall mechanical behavior of composite laminates, and predicting the onset of steam pressure-induced delamination. Investigations on the effect of steam blistering on the degradation of interfacial shear strength, especially for BMI composites, are very rare.

Over decades, a number of experimental techniques have been developed to evaluate the fiber/matrix interface adhesion by mechanically characterizing the interfacial shear strength (IFSS) [13]. IFSS is commonly measured using micromechanical test methods such as the single-fiber fragmentation test [14], the microbond test [15–17], the single-fiber push-out test [18, 19], and the fiber push-in test [20–22]. Yang et al. [16] measured IFSS of thermal-oxidative degradation glass fiber-polypropylene composites by microbond test. Yu et al. [7] reported long-term moisture effects on IFSS measured by microbond test. Micrbond test utilize single fibers embedded in a matrix, such a single fiber model composite is inherently different from actual processed composites. To study the environment effects such as thermal oxidation and steam blistering, it is necessary to measure IFSS on actual composites, in which case fiber push-out and fiber push-in tests can be applied. However, the fiber push-out test requires the cumbersome preparation of very thin sample (~50 μm), and samples tend to break easily during the polishing, which results in extremely low yield in sample preparation. Due to these reasons, the fiber push-in experiments are conducted in this investigation. To the best of our knowledge, for IM7/BMI composites, there have been no results reported on the effect of thermal oxidization and steam blistering, with an emphasis on fiber/matrix interface behavior.

During a fiber push-in nanoindentation experiment, the flat punch tip is pressing on an individual fiber until fiber/matrix interface debonding occurrs. The applied nanoindentation load and the resulting nanoindentation displacement are recorded. A typical push-in nanoindentation load-displacement curve follows an "S" shape [23]. The initial nonlinear region at small depths, designated as "toe" region, is the result of imperfect contact between the fiber and flat punch indenter. As the flat punch tip makes full contact with the fiber end, the resulting push-in load follows a linear relationship with the displacement, giving a contact stiffness S_0, representing linear elastic deformation of fiber and matrix. The end of the linear region marks with the beginning of the fiber/matrix interface failure, or debonding. A simplified shear-lag model [20–25] gives the expression for the interfacial shear strength, τ_0^{SL}

$$\tau_0^{SL} = \frac{S_0 P_C}{2\pi^2 r^3 E_f} \tag{1}$$

where S_0 is the stiffness (slope) of the linear elastic region, P_c is the critical load at the onset of nonlinearity, r is the fiber radius, E_f is the longitudinal elastic modulus of the fiber. The stiffness of the elastic region S_0 depends on the fiber and matrix properties, as well as the confinement from the surrounding fiber and matrix, which depends on the local fiber volume fraction. Rodríguez et al. [21] performed a series of numerical simulations, and reported that the above shear-lag model underestimated interfacial shear strength for push-in experiments conducted at the central fiber of highly-packed clusters with hexagonal symmetry and proposed a simple relationship to provide a correction. However, the relationship reported in [21] is based on fiber and matrix properties of one composite with specific compound and fiber/matrix configurations. The relationship does not necessarily hold for the IM7/BMI composite used in this investigation. Thus, for IM7/BMI composites used in this study, numerical simulations are conducted to assist the determination of interfacial shear strength.

In this paper, unidirectional IM7/BMI composite is exposed to thermo-oxidation at elevated temperatures (195 °C and 245 °C), close to and above the service temperature for 2 months. IM7/BMI laminates are also immersed in water for 2 years at room temperature. The moisture-saturated specimens are heated to 260 °C under a gradual temperature increase or a sudden temperature exposure, and the interfacial shear strength is characterized by fiber push-in nanoindentation. The effect of thermal oxidation and steam blistering is then investigated and discussed in detail.

Material and Experiments

Material

The thermal oxidized unidirectional IM7/BMI composite plates are the same as those used in our work published earlier [5], thus only a brief description on specimen preparation is presented here. The composite square plates with a nominal thickness of 2.0 mm and a side length of 150 mm, are oxidized at 195 °C (close to the service temperature of 204 °C) and at 245 °C (higher than the service temperature but lower than glass transition temperature of 270 °C) in air, respectively for 1500 h (about 2 months). After 1500 h of oxidation, the central portion (at least 41 mm away from all edges) of the large composite plates are cut into small rectangular specimens using 0.3 mm thick diamond-coated saw blade under cooling by flowing water. Subsequently, the specimens are washed, cleaned, and dried at 60 °C for 72 h. A schematic diagram of a unidirectional IM7/BMI composite specimen prepared from a composite panel after oxidation is shown in Fig. 1.

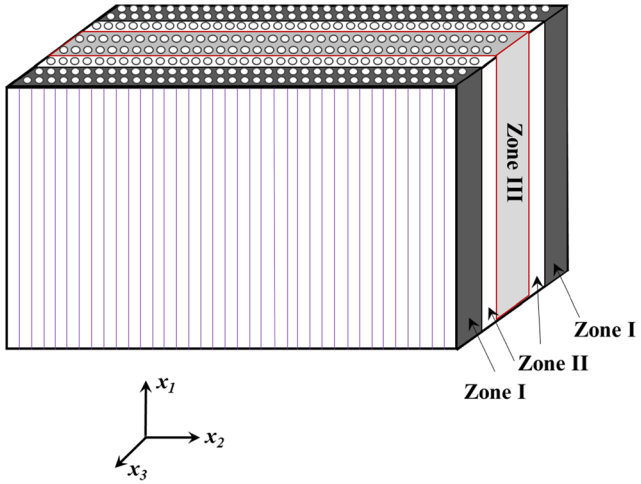

Fig. 1 Schematic diagram of a thermally oxidized IM7/BMI unidirectional composite laminate after exposure to a high temperature. The schematic diagram shows a central portion of a larger laminate after oxidation. The oxidized composite contains three zones: Zone I (fully oxidized zone), Zone II (active reaction zone), and Zone III (unoxidized zone). A Cartesian frame is also shown, with x_1 aligned with fiber direction

To investigate the effect of steam blistering, 6 pieces of unidirectional IM7/BMI composite plates of 38.1 mm wide and 127.0 mm long are cut from composite plates with a thickness of 2.0 mm and 304.8 mm side-length, the samples are immersed in water for nearly 2 years at room temperature. The mass of each plate is weighed by a digital balance (Denver Instrument, APX-200). Before weighing, the plate specimens are removed from water, dried with tissues until a new dry tissue could not absorb any water. The average weight gain is 0.787% in 1.5 years and no additional weight gain is detected thereafter, indicating that it took about 1.5 year to reach a water saturated state. A 0.3 mm thick diamond-coated blade saw is used to cut the specimens. After cutting, the cutting surfaces are lightly polished by #600 sandpaper to produce smooth surface. Subsequently, the specimens are washed, ultra-sonically cleaned, and then placed back into water. Two heating procedures, namely sudden heating (causing a thermal shock) and gradual heating, are used. In the first procedure, a specimen is directly placed inside an oven preheated to 260°C. In the second procedure, the temperature is gradually ramped up to 260°C at a rate of approximately 6°C/min in a Fisher Scientific oven LB 305745 M (320°C maximum temperature with ±2°C accuracy).

For gradual heating, it took 40 min to increase the temperature to 260°C at a rate of approximately 6°C/min. The final average weight loss is 0.760%. However, for the sudden heating, the wet sample is directly placed inside the oven preheated to 260°C for 5 min; and the average final weight loss of a specimen is 0.727%.

The unidirectional IM7/BMI composite specimens are prepared in six conditions, namely (1) baseline specimens, (2) specimens oxidized at 195°C, (3) specimens oxidized at 245°C, (4) wet specimens (fully saturated, and no steam blistering), (5) saturated specimens undergoing sudden heating history to 260°C, and (6) saturated specimens undergoing gradual ramp heating history to 260°C. The composite specimens are embedded into epoxy potting material (modified Bisphenol A-Epichlorohydin Epoxy, Allied High Tech Products, Inc.). Each potted sample is cured at room temperature for 24 h. The cross section perpendicular to the fibers of the unidirectional composite specimens are polished first by #800 and #1200 sandpaper, respectively. The specimens are then polished by a MultiPrep™ system polishing machine using alumina suspension with particle size from 1 μm to 50 nm in sequence. Typical scanning electron microscopic (SEM) images of the cross-sectional area of a baseline specimen are shown in Fig. 2. Most of the cross sections of the IM7 fibers are found to have an approximately circular shape, and

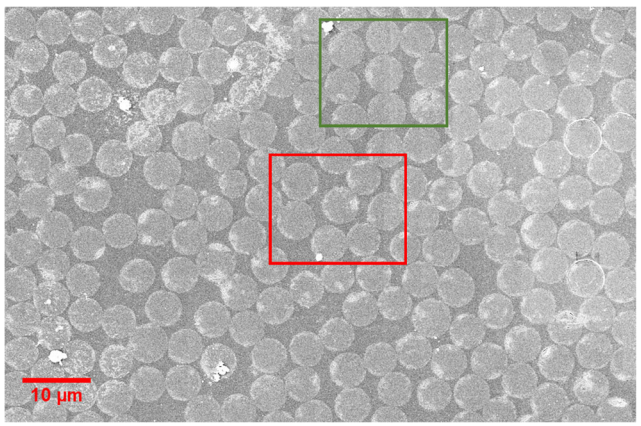

Fig. 2 Scanning electron micrograph of a cross-section of a pristine IM7/BMI composite. The highlighted regions in the red and green boxes are used in full 3D finite element simulations (shown in Fig. 8)

the plane parallel to the specimen surfaces can thus be considered to be perpendicular to the fiber. This plane is used for fiber push-in nanoindentation in the fiber directions.

Fiber Push-in Nanoindentation

In this paper, interfacial shear strength is determined by fiber push-in nanoindentation experiments [20, 21, 23]. All the fiber push-in nanoindentation experiments are conducted on an Agilent G200 nanoindentation system. The nanoindentation system can reach a maximum indentation depth of 500 μm (0.2 nm resolution) and a maximum load of 500 mN (50 nN resolution). A flat punch tip (Micro Star Tech) of 3 μm in diameter is used in this investigation. In order to conduct nanoindentation on an IM7 carbon fiber (5 μm in diameter) at close to the center of a fiber as possible, calibration is conducted to obtain an accurate lateral position of the indenter relative to the sample surface with the use of an optical microscope on the nanoindentation system. All the fiber push-in nanoindentation are conducted at a constant loading rate of 1 mN/s. Considering the fact that the 45^{o} cone angle of indenter used in this investigation, the flat punch tip does not touch the matrix if the maximum displacement is below 1 μm. In this study, the maximum load is chosen such that the maximum nanoindentation displacement is below 700 nm. Twenty-five fiber push-in nanoindentation experiments are conducted for each preparation condition of the IM7/BMI composite specimen. During the experiment, it is found that error in positioning of the flat punch indenter is accumulated over time, making it difficult to push the target fiber right at the center. Thus, the residual indents are checked every five push-in experiments, if the nanoindentation site is off from the center by more than 1 μm, the data is disregarded and the calibration between flat punch tip and optical microscope is re-conducted. The procedure mentioned above is repeated until 25 fiber push-in nanoindentation experiments are completed, with all the nanoindentation sites located approximately in the center of IM7 carbon fibers. Attempts are made to select target fibers that have approximately the same diameter and local fiber configurations, which best represent the overall volume fraction. Fibers selected in experiments are nearly hexagonally packed, and they are not touching the surrounding fibers.

Finite Element Model

General Model

The shear-lag model is used to determine the interfacial shear strength from the push-in nanoindentation on the composites. To this end, finite element method (FEM) is used to simulate the fiber push-in experiments on IM7/BMI composite. The commercial software package ABAQUS V6.14 is used for the modeling. A typical three-dimensional (3D) FEM model, used to simulate the fiber push-in nanoindentation, is shown in Fig. 3. The baseline case of a 3D FEM model is simplified as one sixth of the entire 3D model to reduce the computational time by considering the hexagonal symmetry of the fiber packing. A flat punch tip, 3 μm in diameter, which is same as the one used in experiments, is modelled as rigid. The central IM7 carbon fiber with 5 μm diameter is surrounded by six IM7 carbon fibers. Those carbon fibers are embedded in the BMI matrix and this central region is surrounded by an annular region of homogeneous material continuum with effective properties of IM7/BMI composite. The height and radius of the FEM model are selected to be 375 and 80 μm, respectively. This model size is found to be large enough to

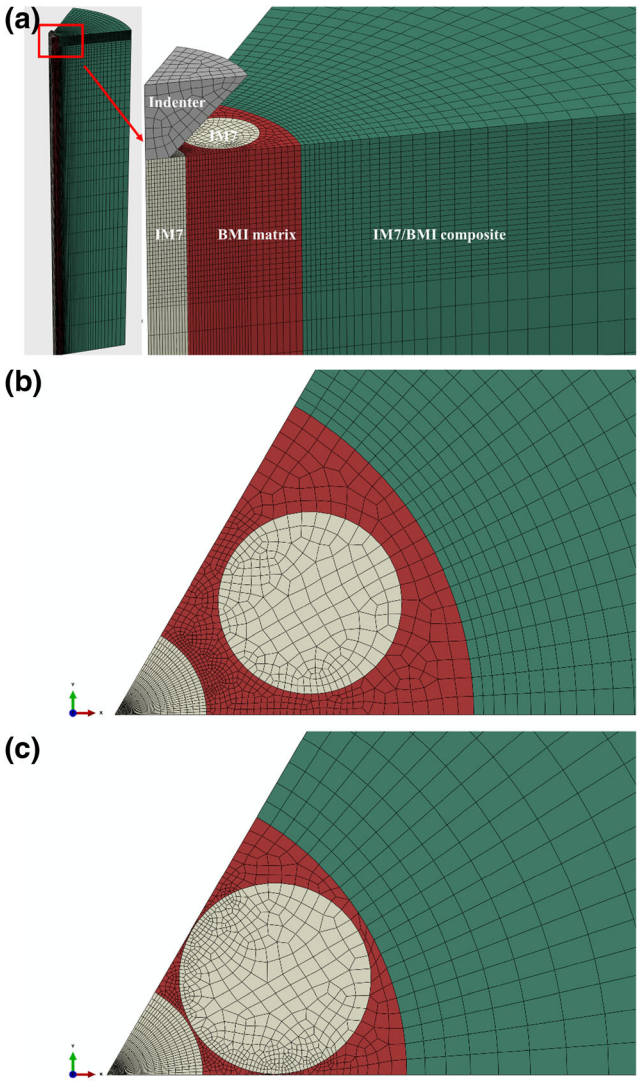

Fig. 3 Three dimensional finite element models for nanoindentation push-in experiment for IM7/BMI composite. **(a)** overall geometry and FEM mesh; **(b)** top surface of the FEM model for pristine composite, with a local fiber volume fraction of 0.6; **(c)** top surface of the FEM model corresponding to a local fiber volume fraction of 0.9

avoid sample size effect on the push-in nanoindentation load-displacement curve. The distance between the central fiber and surrounding fiber is specified such that it corresponds to a 60% fiber volume fraction. It is found that the local fiber arrangement used in this investigation agreed well with the experimental results. The validity of this assumption is addressed in the Discussion section, below.

The carbon fiber is modeled as a transversely isotropic and linear elastic solid, and the BMI matrix is modeled as a linear elastic isotropic solid. Material properties used in simulations are taken from previously published data [26, 27], as summarized in Table 1. The yield strength of BMI matrix is above 200 MPa [28], which is several times larger than the interfacial shear strength. Since the yield strength is twice as large as the interfacial shear strength, plastic deformation of the matrix is not taken into account in this investigation, assuming linear elastic response of BMI matrix does not affect the onset of nonlinearity, and the results on the interfacial shear strength [21, 29]. In the FEM models, different parameters are considered, these include: interfacial strength, interfacial fracture energy, local fiber arrangement, curing residual stresses, and friction coefficient. The FEM model contains 117,422 linear hexahedral fully-integrated elements (C3D8) and 2010 linear wedge fully-integrated elements (C3D6). Adaptive meshing is used, and very fine mesh is used at the fiber/matrix interface and the region underneath the flat punch indenter. The fiber/matrix interface is considered as infinitesimally thin, and a surface-based cohesive interactions are used in the model to take into account the fiber/matrix debonding and the effect of friction during fiber push-in nanoindentation. Mesh convergence studies are conducted to ensure that mesh independence is achieved.

Surface-Based Cohesive Behavior

To model the debonding between fiber and matrix, a surface-based cohesive interaction is used and the interface is assumed to satisfy the bilinear traction separation law. The undamaged and uncoupled linear elastic traction separation behavior is defined as,

$$\mathbf{t}=\begin{Bmatrix} t_n \\ t_s \\ t_t \end{Bmatrix} = \begin{bmatrix} K_{nn} & 0 & 0 \\ 0 & K_{ss} & 0 \\ 0 & 0 & K_{tt} \end{bmatrix} \begin{Bmatrix} \delta_n \\ \delta_s \\ \delta_t \end{Bmatrix} = \mathbf{K}\boldsymbol{\delta} \tag{2}$$

where **t** is nominal traction vector and $\boldsymbol{\delta}$ is separation displacement vector. **K** is stiffness matrix. The subscripts n, s, and t represent normal, shear and tangential components at the fiber/matrix interface, respectively. Damage is initiated once the quadratic traction criterion is satisfied,

$$\left\{\frac{\langle t_n \rangle}{t_n^0}\right\}^2 + \left\{\frac{t_s}{t_s^0}\right\}^2 + \left\{\frac{t_t}{t_t^0}\right\}^2 = 1 \tag{3}$$

where t_n^0, t_s^0 and t_t^0 are normal, shear, and tangential interfacial strength, respectively. Brackets for t_n are the Macaulay brackets, which return the argument if it is positive and give a zero if the argument is negative, since the compressive normal stresses will not open the crack [15, 21, 30]. It is noted that the fiber push-in nanoindentation only provide the values of the interfacial shear strength. In this study, isotropic interfacial strengths are assumed, specifically $t_n^0 = t_s^0 = t_t^0 = \tau_0$. The cohesive behavior is defined to follow the linear softening damage evolution law,

$$\mathbf{t}=(1-D)\mathbf{K}\boldsymbol{\delta} \tag{4}$$

where D is the damage parameter defined as 0 in the case of no damage and 1 at the complete failure. Additional details on the bilinear traction separation law can be found in the literature [15].

In this investigation, a series of simulations are conducted by varying interfacial shear strength, τ_0 = 40, 50, 60, 70, 80, 90 and 100 MPa; interfacial fracture energy, G_c = 2, 5, 10, 20, 30, 40 and 80 J/m^2; friction coefficient, μ = 0, 0.2, 0.4 and 0.6. To study the effect of residual stress induced in the curing process, isotropic coefficient of thermal expansion for the BMI matrix, and anisotropic coefficients of thermal expansion for IM7 fiber and IM7/BMI composite are used, with values given in Table 1. An initial stress state is introduced based on a cooling from the curing temperature of 227 °C to room temperature. The conclusions obtained from the above simulations are used to interpret the experimental data.

Table 1 Material properties used in FEM simulations

Material property		IM7 fiber	IM7/BMI composite	BMI matrix
Longitudinal modulus	E_1 (GPa)	276	174	4.6
Transverse modulus	E_2 (GPa)	19	12.1	
Shear modulus	G_{12} (GPa)	27	9.0	
Poisson's ratio	ν_{12}	0.2	0.36	0.35
Poisson's ratio	ν_{23}	0.2	0.45	
Longitudinal CTE	α_1 (10^{-6}/°C)	−0.4	0.25	44
Transverse CTE	α_2 (10^{-6}/°C)	5.6	21.1	

Results and Discussions

Fiber Push-in Nanoindentation and FEM Simulations: Baseline Specimens

Fiber push-in nanoindentation experiments are conducted first on pristine IM7/BMI composite, and the experimental load-displacement curves are shown in Fig. 4, from which a reasonably good reproducibility can be observed. The experimental load-displacement curves are also compared with simulated curves. They agree with each other reasonably well, especially in the linear region, indicating that our FEM model with a fiber volume fraction of 60%, both for overall composite, and for local region can capture the mechanical behavior of IM7/BMI composite during the fiber push-in nanoindentation. For a detailed microscopic analysis of the load-displacement relationship, fiber push-in nanoindentation is paused at different loading stages, and unloaded. SEM micrographs of the push-in fibers are acquired to illustrate the deformation process, as shown in Fig. 5. By increasing the load, stress at the fiber/matrix interface increases. At the stage corresponding to the nanoindentation depth of approximately 150 nm (Fig. 5(a)), there is an initiation of fiber/matrix debonding, as pointed by the white arrow. As nanoindentation depth reaches nearly 250 nm, the crack propagation results in a larger region of debonding between fiber and matrix, as shown in Fig. 5(b). Finally, when the nanoindentation depth is close to 400 nm, fiber has fully debonded from the matrix, as shown in Fig. 5(c) and (d). SEM micrographs confirm that the indenter tip makes contact with the fiber only and does not touch the surrounding matrix region. In some situations, partial debonding also occurs in the neighboring fibers

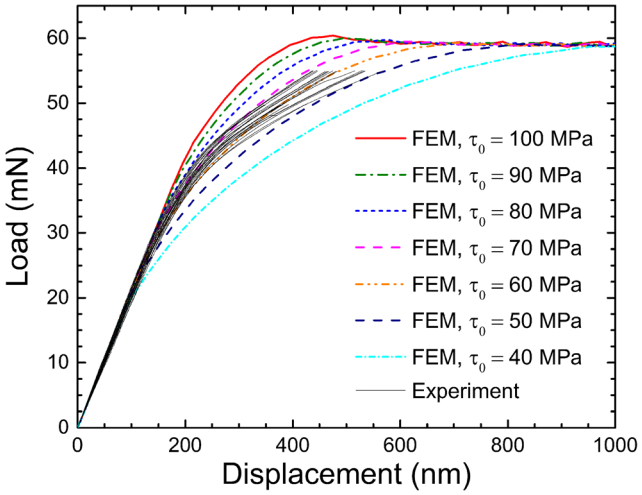

Fig. 4 Nanoindentation push-in experimental and simulated load-displacement curves for IM7/BMI pristine specimen. Black lines represent the experimental results, other color curves are FEM simulation results with different input values for the interfacial shear strength

(Fig. 5(d)). Following this observation, cohesive interaction between neighboring fibers and BMI matrix is also included in our FEM simulations. The debonding in neighboring fibers is successfully captured by our FEM model, the details of which are presented below.

In order to determine the interfacial shear strength accurately from experimental load-displacement curves, a series of FEM simulations are conducted to study the effects of interfacial shear strength, interfacial fracture energy, friction between fiber matrix, and residual stress induced in curing process. By doing so, the shear-lag model (equation (1)) is examined by comparing results with FEM simulations, the

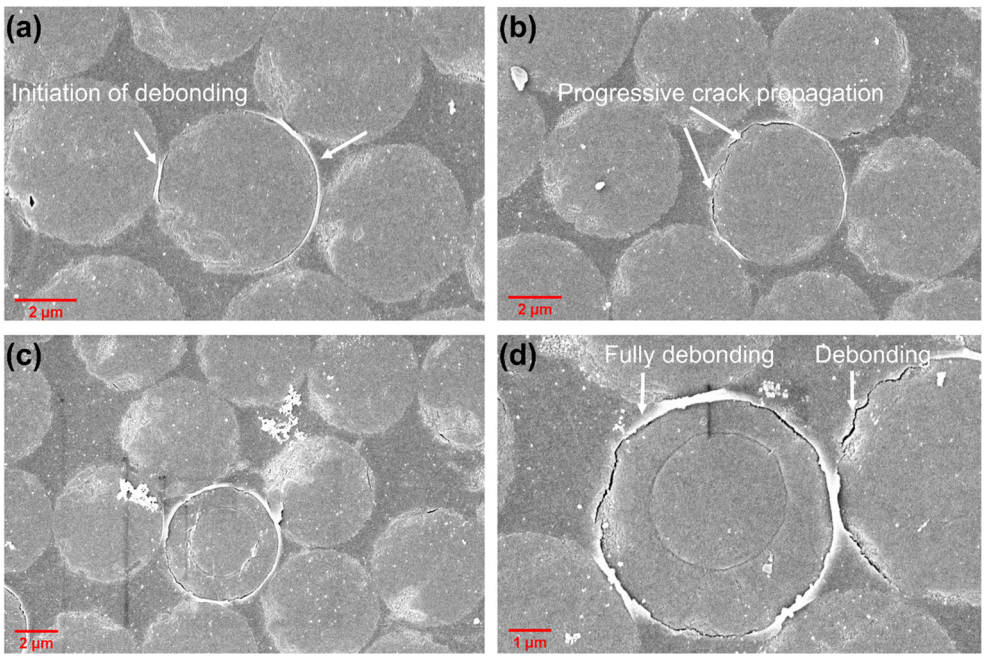

Fig. 5 SEM images of sample surfaces after interruption at different loading stages during the fiber push-in experiments. (**a**) experiment paused at nearly 150 nm nanoindentation depth: initiation of fiber/matrix debonding; (**b**) experiment paused at approximately 250 nm nanoindentation depth: progression of the fiber/matrix debonding; (**c**) experiment paused at nearly 400 nm nanoindentation depth: fully fiber/matrix debonding; (**d**) another experiment paused at nearly 400 nm nanoindentation depth: fully fiber/matrix debonding, the debonding was also observed at a neighboring fiber

comparison indicates that the shear-lag model is applicable to the experimental fiber push-in configuration of IM7/BMI composites used in this investigation. For the first set of fiber push-in simulations, friction and curing residual stresses are neglected, and all the fiber/matrix interfaces are assumed to have the identical interfacial fracture energy G_c of 20 J/m^2. To perform a parametric sensitivity study, different interfacial shear strengths are assigned in the FEM model, which fall in the typical range of interfacial shear strength of carbon fiber reinforced polymer composites: 40, 50, 60, 70, 80, 90 and 100 MPa, respectively. The corresponding load-displacement curves predicated by FEM are shown in Fig. 6(a), it is found that all the curves have the same initial slope, followed by a non-linear region, and a plateau region with constant load, corresponding to the propagation of the interface crack from the upper surface, and steady-state situation of crack propagation, respectively. Further, the lower the assigned interfacial shear strength, the lower is the onset of nonlinearity. The behavior experienced here is very similar to those reported in previous work [21]. Those results are not surprising since the initial slope is governed by the geometry configuration and elastic properties of the fiber and matrix. The constant load at steady-state is controlled by the interface fracture energy, as shown in Fig. 6(b).

The push-in nanoindentation load-displacement curves in Fig. 6(b) are collected from the second series of FEM simulation by varying G_c = 2, 5, 10, 20, 30, 40 and 80 J/m^2 while interfacial shear strength is kept at a constant value of 60 MPa. It is concluded that the values for interfacial fracture energy does not affect the onset of nonlinearity, thus confirming that the calculation of interfacial shear strength is independent of interfacial fracture energy, for fiber push-in nanoindentation [21].

Effects of friction and curing residual stresses are also examined. FEM simulations are conducted with different values of the friction coefficient, specifically, 0, 0.2, 0.4, and 0.6. An initial stress state is introduced based on a cooling from the curing temperature of 227 °C to room temperature. In this set of FEM simulations, interfacial shear strength and interfacial fracture energy are given as 60 MPa and 20 J/m^2, respectively. The corresponding load-displacement curves are shown in Fig. 6(c). It is found that friction increases the interfacial shear resistance [21, 31], and residual compressive stresses due to curing further enhance the interfacial shear resistance which is due to the added friction resulting from the residual compressive stresses. The onset of nonlinearity is not affected by the existence of friction [21] and thermal residual stresses [31], thus the calculation of interfacial shear strength are unlikely to be affected by these parameters.

FEM simulations are also conducted to take into account of the configuration with extremely high local fiber volume fraction (V_f = 0.9). Figure 3(c) shows the FEM mesh of the top surface, this model is very similar to the configuration in reference [21]. For this case, interfacial fracture energy is

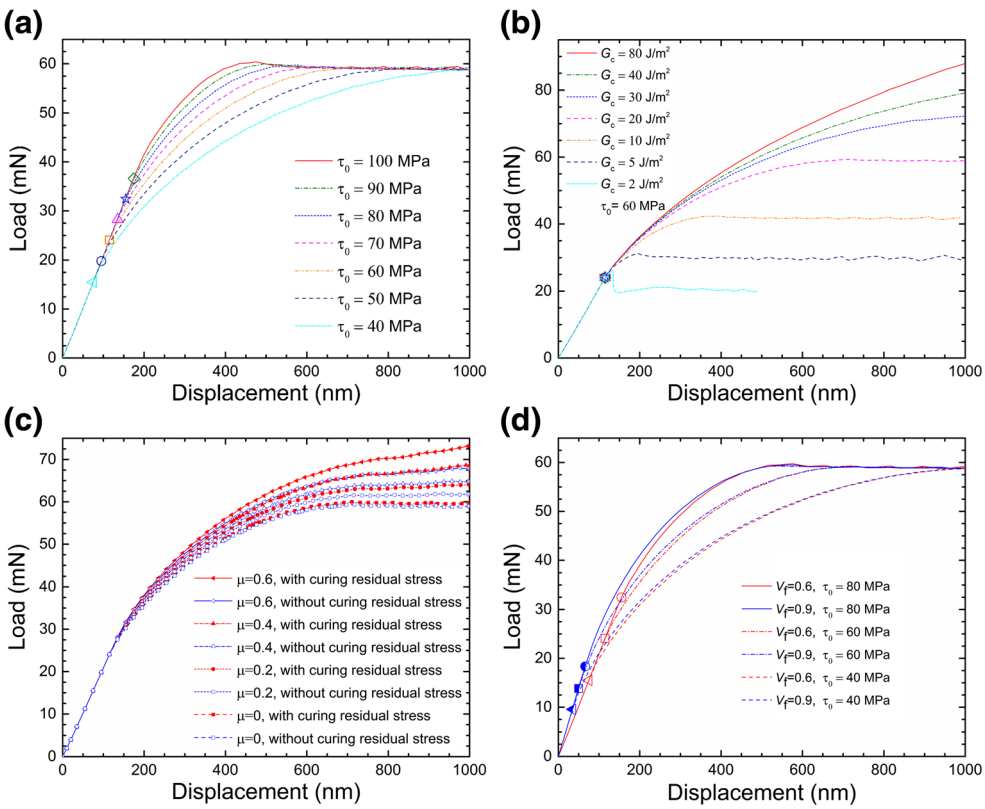

Fig. 6 FEM simulated nanoindentation push-in load-displacement curves for pristine composite. (**a**) curves showing the effect of interfacial shear strength, the onset of fiber/matrix debonding is marked with different symbols; (**b**) effect of interfacial fracture energy; (**c**) effect of curing residual stress and friction coefficient; (**d**) effect of local fiber volume fraction

assumed to be 20 J/m^2 and interfacial shear strength is 40, 60, and 80 MPa, respectively. It is assumed that no friction and residual thermal stress exist. Load-displacement curves obtained from the above model are compared with baseline FEM model ($V_f = 0.6$), shown in Fig. 6(d). The initial stiffness increases as the local fiber volume fraction becomes larger, while the critical load at onset of nonlinearity remains lower.

Debonding of the neighboring fiber is also investigated using this model. The interfacial shear strength is set to be 40, 80, and 100 MPa, respectively, and interface fracture energy is assumed to be 20 J/m^2. The interface properties are assumed to be the same for both cohesive surfaces, namely central fiber/matrix and neighboring fiber/matrix. As shown in Fig. 7(a) and (b), cohesive interaction between neighboring fiber and matrix has negligible effect on the overall load-displacement relationships. Differences are only observed in the steady-state crack propagation region. Figure 7(c) and (d) indicate that initiation and propagation of debonding at the neighboring fiber/matrix interface does occur. Debonding occurs in the region close to the central fiber. This agrees with the observation in experimental results shown in Fig. 5(d).

Equation (1) is used to calculate the interfacial shear strength. It is found that the shear-lag model underestimates the local constraint effect for $V_f = 0.9$ FEM model, and an empirical correction coefficient 1.32 could be used for such a model, with the consideration of IM7/BMI composite material properties.

The strategy proposed in Rodríguez et al. [21], takes advantage of the fact that a central fiber is surrounded by six fibers in a perfect hexagonal packing ($V_f = 0.9$ locally). This can be often found in composites with large fiber volume fraction. By properly selecting target fibers with a very close hexagonal packaging, fiber push-in nanoindentation can be conducted on the central fibers subjected to the same constraint from the nearest-neighbor fibers, and thus reduce the experimental uncertainty. However, an empirical correction coefficient has to be used. The correction factor is not universal, and depends on the geometry configuration and constitutive behavior of fiber, matrix and surrounding composites. More details can be found in the work by Rodríguez et al. [21], where the correction coefficient is 1.92 in their case.

In this investigation, the FEM model with $V_f = 0.6$ is chosen as the baseline model for the following reasons: First, in contrast to $V_f = 0.9$ FEM model, for FEM model with $V_f = 0.6$, interfacial shear strength calculated by equation (1) is very close to the interfacial shear strength assigned. This is due to the fact that, the shear-lag model works very well if the surrounding fiber constraint is not high and a correction factor is

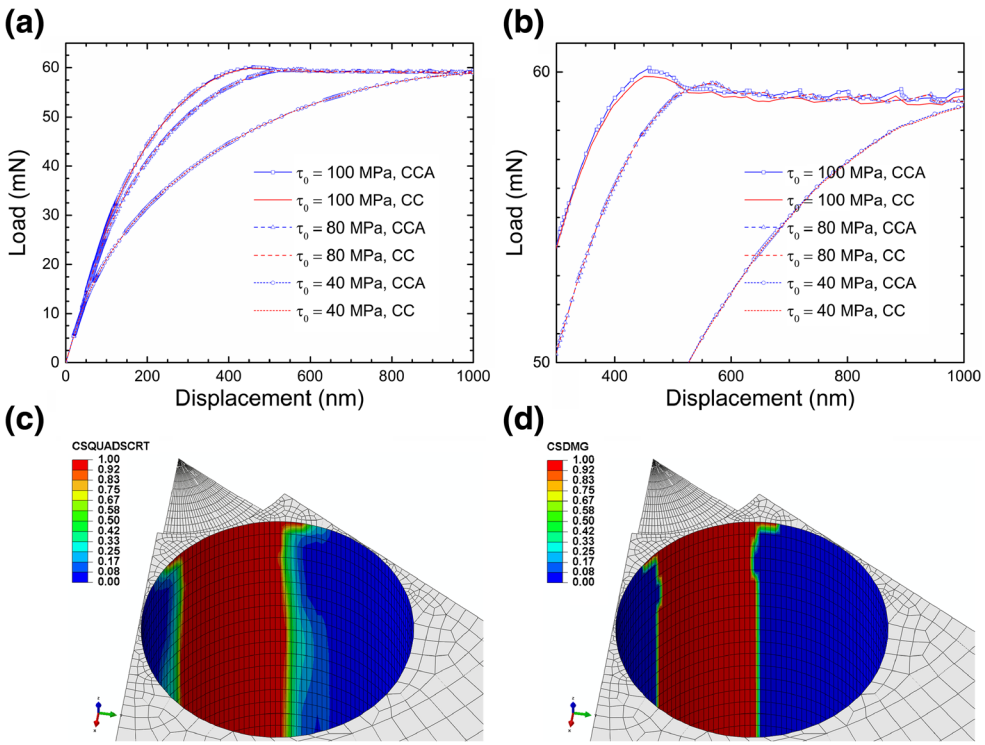

Fig. 7 FEM simulation of fiber push-in experiments, cohesive interfaces were considered between neighboring fibers and matrix (**a**) nanoindentation push-in load-displacement curves. "CCA" represents "Cohesive surfaces exist in Central fiber/matrix and Adjunct fiber/matrix region. "CC" represents "Cohesive surface only exist in central fiber/matrix region; (**b**) enlarged figure of nanoindentation push-in load-displacement curve, a slight difference is observed in the steady-state crack propagation region; (**c**) contour plot of the damage initiation parameter (CSQUADSCRT) of the cohesive surface; the red region corresponds to the initiation of fiber/matrix debonding; (**d**) damage parameter of the cohesive surface; the red region represents fully-debonded fiber/matrix interface. The fiber/matrix debonding region in the neighboring fiber is the closest to the central fiber

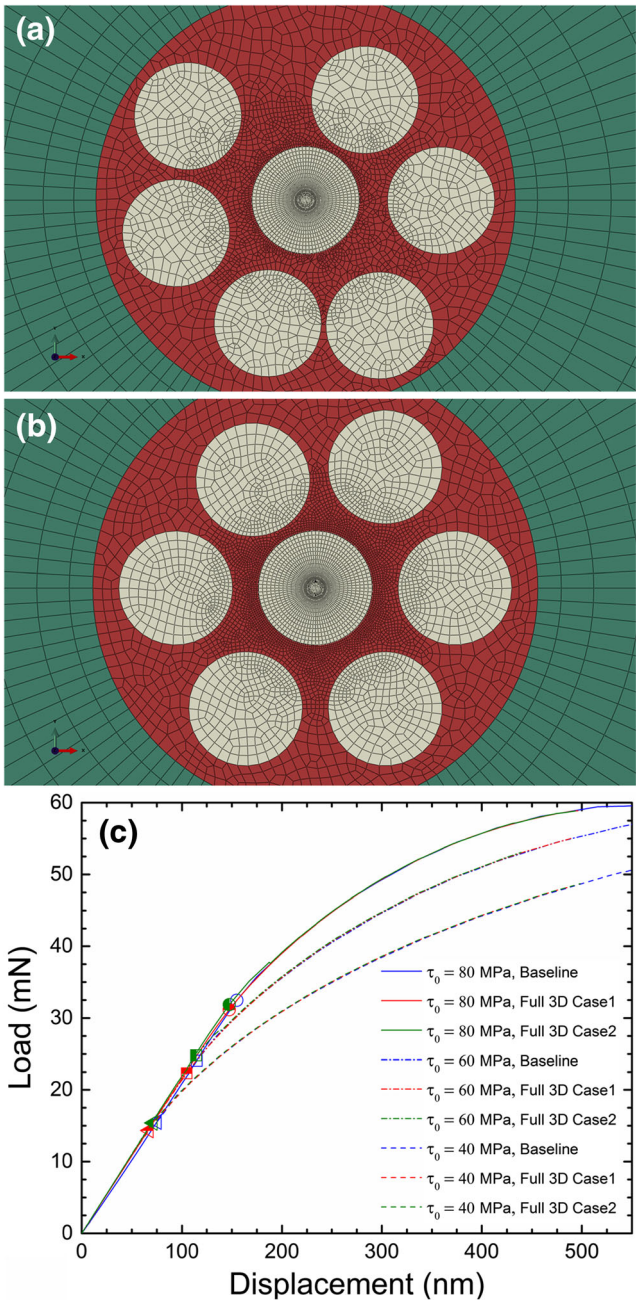

Fig. 8 FEM simulation results for fiber push-in experiments. Full 3D FEM models were considered. (**a**) local fiber arrangement of Case 1, surface information was taken from the red box in Fig. 2; (**b**) local fiber arrangement of Case 2, surface information was taken from green box in Fig. 2; (**c**) push-in load-displacement curves

not needed. Second, as shown in Fig. 4, a very good agreement is reached between experiments and $V_f = 0.6$ FEM model, particularly on the initial stiffness part. In the case where equation (1) is not used, inverse method could be used to allow the simulation curves to agree with experimental data, by adjusting the interface properties. Such an inverse calculation method is not possible for our $V_f = 0.9$ model, since the initial slope of load-displacement curve does not change by modifying interface properties only. Last, but not least, a highly packed hexagonal central fiber can be found in IM7/BMI composites. However, it is usually asymmetric, which can be seen in Figs. 2 and 5. It is noted that both $V_f = 0.9$ and $V_f = 0.6$ FEM simulations only consider the central fiber and 6 fibers around, while the surrounding area is assumed to behave as bulk composite. Recently, Jäger et al. [30] and Naya et al. [32] used a larger RVE, taken from cross-section micrograph, in their FEM simulation. When such a RVE is used, the fiber volume fraction in the central part (multiple fibers surrounded by matrix) is comparable to fiber volume fraction of the bulk composites. This method reflects the real situation, but is much more computationally expensive [30, 32].

It is observed that there is a slight uncertainty in the experimental load-displacement curve. This uncertainty can be attributed to the varying surrounding environment of the analyzed fibers and/or deviation of nanoindentation site from the center of the IM7 fiber. The baseline FEM model is established under the assumption of symmetric loading and geometry. Two non-symmetric configurations are simulated, as shown in Fig. 8. The entire 3D model is simulated due to the loss of symmetry. There are 425,650 and 435,351 elements, respectively. The fiber arrangement in the central region is taken from the SEM micrograph, as shown in Fig. 2. It is seen that both the critical load and the slope of nanoindentation load-displacement curves of these two configurations are slightly different with the baseline FEM model. However, IFSS calculated by shear-lag model is fairly accurate.

Due to the reasons mentioned above, it is determined to use the $V_f = 0.6$ model as the baseline simulation model. Even though there is a slight underestimation of interfacial shear strength for some extreme cases, namely a lot of fibers highly hexagonally-packed together, the interfacial shear strength obtained in this study can be at least considered as lower bound. In our sample, such extreme geometries were rare, and we avoided them in our testing.

Effect of Thermal Oxidation on Interfacial Shear Strength

After the composite specimens are exposed to isothermal oxidation for 1500 h, a larger reduction in interfacial shear strength is measured for specimens isothermally oxidized at 245 °C than at 195 °C. These specimens are cut from areas of the oxidized plates far away from the edges [5].

Oxidation occurs primarily along the thickness, which is the x_3- direction identified in Fig. 1. Three oxidation zones from the surface to the core of a unidirectional composite specimen [5, 33] are identified as zone I, zone II, and zone III. Oxygen is diffused from the atmosphere into the surface layer to form oxidized and damaged zone I. Zone II is the active oxidation process zone, which is the transition region between zone I and zone III. Zone III is in the central core

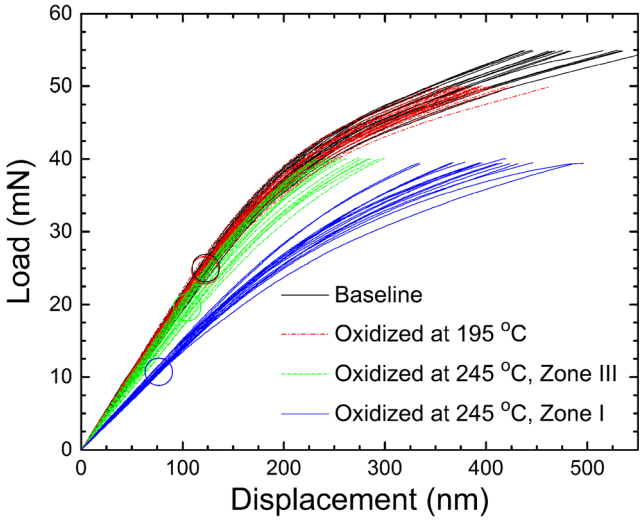

Fig. 9 Experimentally obtained nanoindentation push-in load-displacement curves for unidirectional IM7/BMI specimen: effect of thermal oxidation

region occupied by material which has not yet been oxidized. It is found that after 2 months of exposure to elevated temperatures, the outer layers of a composite panel have been thermally oxidized while the interior is thermally aged but not necessarily oxidized. In this study, fiber push-in experiments are conducted on zone I (close to the edge of the specimens) and zone III (close to the center of the specimens).

Figure 9 shows the load-displacement curves from fiber push-in nanoindentation on different specimens, namely (1) baseline specimens, (2) specimens oxidized at 195°C, (3) specimens oxidized at 245°C from zone III, and specimens oxidized at 245°C from zone I. In Fig. 9, the initial nonlinear region is removed, in other words, toe correction at small displacement has been made on these curves following the ASTM Standard D695–15. Equation (1) uses linear slope of the load-displacement curve, which is outside of the toe region. Figure 9 indicates that the change of slope and critical load are not apparent for specimens oxidized at 195°C. However, for specimens oxidized at 245°C, both the linear slope and critical load exhibited significant reduction, especially in zone I.

To determine the interfacial shear strength, it is important to accurately identify the critical load at the onset of nonlinearity of load-displacement curve. The algorithm for seeking the onset of nonlinearity is briefly introduced here: the data point between 0 mN and 10 mN is used to obtain an average slope. For every data point thereafter, the slope is compared with the average slope. If the difference is larger than 0.5%, the data point is marked as a "suspect" point. The 30 data points following the "suspect" point are checked to compare the slope with the average slope. If any slope from these 30 data points is same or within 0.5% difference compared with the average slope, the "suspect" point is disregard. Otherwise, the "suspect" point is marked as "critical" point. The above iteration continues until the critical load is found. The algorithm mentioned above is implemented in a MATLAB routine. The MATLAB routine is checked and verified with FEM simulations curves to ensure its accuracy. It is, then, applied to experimental load-displacement curves to determine the critical load.

Table 2 Summary of interfacial shear strength of IM7/BMI composite in different conditions

Samples	Interfacial shear strength (MPa)	Percentage of reduction (%)
Baseline	58.3±3.7	–
Oxidized at 195 °C	57.5± 4.9	1.4
Oxidized at 245 °C, Zone III	47.4 ± 4.3	18.7
Oxidized at 245 °C, Zone I	20.6 ± 3.5	64.7
Water immersion for 2 year	56.7±2.9	2.7
Ramp heating	57.1 ± 3.7	2.1
Step heating	47.7 ± 2.8	18.2

The interfacial shear strength determined by fiber push-in nanoindentation is summarized in Table 2 (the first four rows of data). The results are compared to the baseline case, and analyzed by Welch's unequal variances t-test [34], as summarized in Table 3. After oxidation for 1500 h at 195 °C, the interfacial shear strength exhibited no reduction compared with baseline (insignificant difference based on statistics), indicating good durability at a service temperature of 195 °C for IM7/BMI composites. After oxidation for 1500 h at 245 °C, the interfacial shear strength in zone III reveals a reduction of 18.7% compared with baseline data. The interfacial shear strength in zone I, however, exhibits a more significant reduction of 64.7%, compared with the baseline. This indicates a significant reduction in durability at a temperature which is 40 °C higher than the service temperature for IM7/BMI composites. The degradation in interfacial strength revealed experimentally provides direct evidence of the marked reduction in

Table 3 Summary of Welch's unequal variances t-test results of interfacial shear strength of IM7/BMI composite in different conditions compared with baseline

Samples	*p*-value	Significantly different from the baseline?
Baseline	–	
Oxidized at 195 °C	0.514	No
Oxidized at 245 °C, Zone III	2.13×10^{-10}	Yes
Oxidized at 245 °C, Zone I	3.53×10^{-28}	Yes
Water immersion for 2 year	0.104	No
Ramp heating	0.332	No
Step heating	2.02×10^{-13}	Yes

Note: *p*-value is the probability for the Welch's unequal variances t-test model that when the null hypothesis is true. The statistical significance level, $\alpha = 0.05$. If *p*-value is smaller than the α, the results are statistically different with baseline

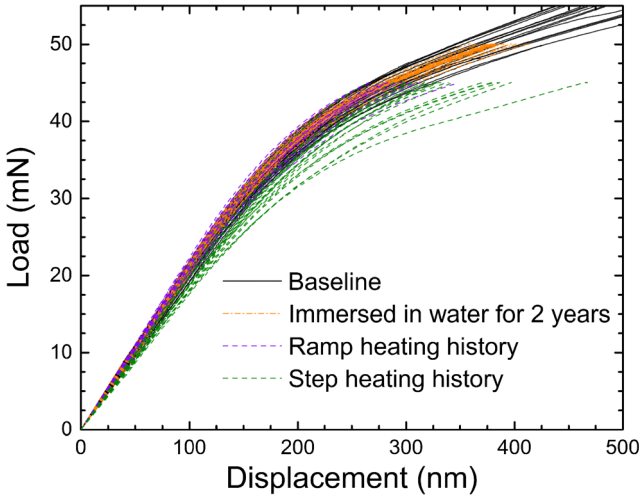

Fig. 10 Experimentally obtained nanoindentation push-in load-displacement curves for unidirectional IM7/BMI composite specimen: effect of steam blistering

compressive stiffness and strength of the composites reported earlier [5].

Effect of Steam Blistering on Interfacial Shear Strength

Fig. 10 shows the load-displacement curves of fiber push-in nanoindentation on different type of specimens, namely (1) baseline, (2) water-immersed, (3) gradually heated, and (4) suddenly heated specimens. It is observed that load-displacement curves obtained from the water-immersed specimens and gradual heating specimens are comparable to baseline. The load-displacement curves obtained from the suddenly heated specimens show reduction in both initial slope and critical load. The interfacial shear strength determined by fiber push-in nanoindentation is summarized in Table 2 (bottom three rows of data). The results are compared to the baseline case, and analyzed by Welch's unequal variances t-test [34], as summarized in Table 3. It is found that there is a negligible reduction (insignificant difference based on statistics) in interfacial shear strength of both water-immersed specimens and gradually heated specimens, compared to the baseline data. A significant reduction (18.2%) in interfacial shear strength is found in the suddenly heated specimens, compared with the baseline. This indicates the fiber/matrix interface of IM7/BMI composites can sustain long-term moisture exposure without appreciable degradation in interfacial shear strength. It also indicates that slow heating will simply dry the IM7/BMI composites while rapid heating may result in large internal water vapor pressures, leading to void nucleation in matrix and at the fiber/matrix interface, which reduces the fiber/matrix interfacial shear strength. The degradation at the interface makes it easier for the initiation and propagation of microcracks, which can potentially lead to global failure of the structural components of an aircraft.

The degradation at the interface is also confirmed by SEM micrographs of IM7/BMI composite specimens, as shown in Fig. 11. Figures 11(a) and (b) are acquired in zone I which is the fully oxidized region of IM7/BMI specimens oxidized at 245 °C. It is observed that microcracks or initiation of debonding exist extensively at fiber/matrix interface, which correlate with the degradation of interfacial shear strength. Figures 11(c) and (d) are used to illustrate the typical surface of IM7/BMI specimens under sudden heating. For some of the fibers, microcracks are clearly observed at the fiber/matrix interface.

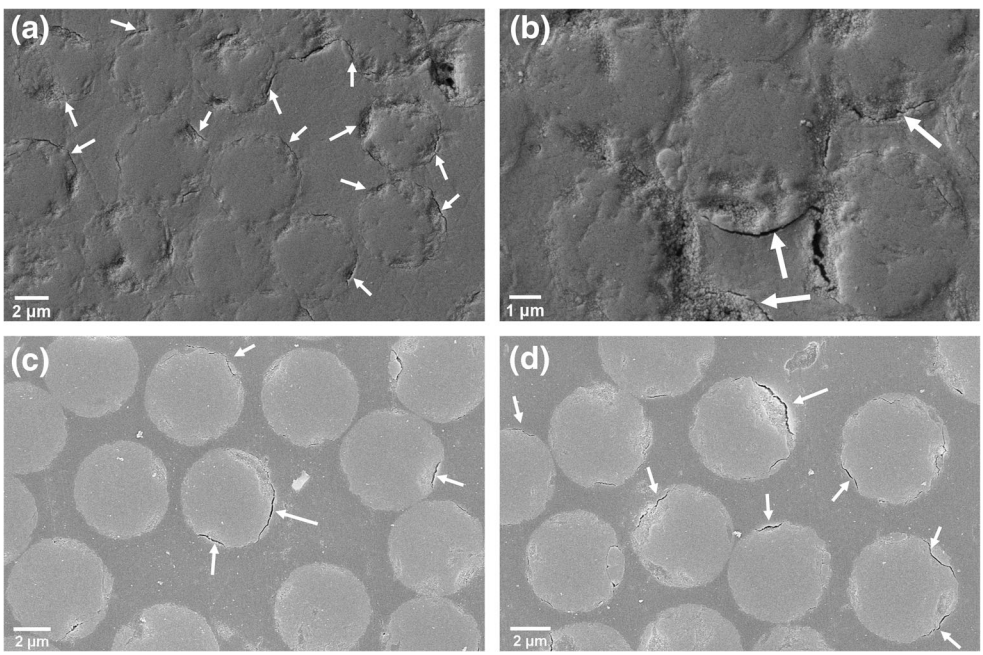

Fig. 11 Typical SEM micrographs of IM7/BMI unidirectional composite sample surfaces. The white arrows point to the pre-existing initial cracks at the fiber/matrix interface **(a)** thermally oxidized zone at 245 °C, fully oxidized region (Zone I); **(b)** enlarged view of thermally oxidized zone at 245 °C, Zone I; **(c)** one region formed after a step heating history; **(d)** another region after a step heating history

Conclusions

Fiber push-in experiments are conducted to evaluate the effects of thermal oxidation and steam blistering on the interface behavior of IM7/BMI unidirectional composite. Systematic FEM simulations with appropriate geometric configuration are performed to validate and justify the fiber-push in experiments. This study illustrates that lower-bound interfacial shear strength can be determined by the shear-lag model regardless of the interfacial fracture energy, residual stresses due to curing process, and friction between fiber and matrix. FEM simulations agree reasonably well with the fiber push-in nano-indentation experiments for baseline specimens.

For composite specimens oxidized at 195 °C for 2 months, the degradation in interfacial shear strength is found to be negligible. For composite specimens oxidized at 245 °C for 2 months, significant degradation is found in interfacial shear strength, specifically 18.7% reduction in central unoxidized zone III and 64.7% reduction in oxidized and damaged zone I. These results provide direct evidence that extensive oxidative degradation of fiber/matrix interfacial shear strength causes easier fiber/matrix debonding and crack growth. This debonding and crack growth are the primary cause of the eventual dynamic compressive failure observed in prior studies.

For composite specimens immersed in water for 2 years, the degradation in interfacial shear strength is found to be negligible, indicating a reasonably good moisture resistance of IM7/BMI composites. Some of these specimens are heated suddenly or gradually to study the effect of steam blistering. It is concluded that gradual heating at a rate of nearly 6°C/min caused slow drying with negligible reduction in interface shear strength. Sudden heating, however, is found to have an 18.2% degradation in interfacial shear strength.

In this investigation, it is evident that extensive thermal oxidation and steam blistering degrade the fiber/matrix bonding, which makes it easier to initiate and propagate microcracks along the interface, potentially leading to global structural failure in aircraft components.

Acknowledgements The support by AFOSR FA9550-14-1-0227, NSF ECCS-1307997 and CMMI-1636306 is acknowledged. Lu also thanks the Louis A. Beecherl Jr., Chair for additional support. We thank Dr. Gregory A. Schoeppner at Air Force Research Lab for providing composites used in this work, and Dr. Dani Fadda for editing the manuscript.

References

1. Morgan RJ, Jurek RJ, Yen A, Donnellan T (1993) Toughening procedures, processing and performance of bismaleimide-carbon fibre composites. Polymer (Guildf) 34:835–842. https://doi.org/10.1016/0032-3861(93)90371-G
2. Morgan RJ, Eugene Shin E, Rosenberg B, Jurek A (1997) Characterization of the cure reactions of bismaleimide composite matrices. Polymer (Guildf) 38:639–646. https://doi.org/10.1016/S0032-3861(96)00542-3
3. Drukker E, Green AK, Marom G (2003) Mechanical and chemical consequences of through thickness thermal gradients in polyimide matrix composite materials. Compos A Appl Sci Manuf 34:125–133. https://doi.org/10.1016/S1359-835X(02)00261-0
4. Ju J, Morgan RJ (2004) Characterization of microcrack development in BMI-carbon fiber composite under stress and thermal cycling. J Compos Mater 38:2007–2024. https://doi.org/10.1177/0021998304044773
5. Luo H, Roy S, Lu H (2012) Dynamic compressive behavior of unidirectional IM7/5250-4 laminate after thermal oxidation. Compos Sci Technol 72:159–166. https://doi.org/10.1016/j.compscitech.2011.10.012
6. Luo H, Lu G, Roy S, Lu H (2013) Characterization of the viscoelastic behavior of bismaleimide resin before and after exposure to high temperatures. Mech Time-Depend Mater 17:369–399. https://doi.org/10.1007/s11043-012-9189-6
7. Yu B, Jiang Z, Yang J (2015) Long-term moisture effects on the interfacial shear strength between surface treated carbon fiber and epoxy matrix. Compos A Appl Sci Manuf 78:311–317. https://doi.org/10.1016/j.compositesa.2015.08.027
8. Bradley W, Grant T (1995) The effect of the moisture absorption on the interfacial strength of polymeric matrix composites. J Mater Sci 30:5537–5542. https://doi.org/10.1007/BF00351570
9. Czabaj MW, Zehnder AT, Chuang KC (2008) Blistering of moisture saturated graphite/polyimide composites due to rapid heating. J Compos Mater 43:153–174. https://doi.org/10.1177/0021998308099323
10. Czabaj MW, Zehnder AT, Hui CY (2010) Delamination of moisture saturated graphite/polyimide composites due to rapid heating. Compos Part B Eng 41:568–577. https://doi.org/10.1016/j.compositesb.2010.05.008
11. Hui C, Muralidharan V, Thompson MO (2005) Steam pressure induced in crack-like cavities in moisture saturated polymer matrix composites during rapid heating. Int J Solids Struct 42:1055–1072. https://doi.org/10.1016/j.ijsolstr.2004.06.058
12. Muralidharan V, Hui CY (2006) Effect of heating rate on steam pressure induced in crack-like cavities in moisture saturated polymer matrix composites. Int J Solids Struct 43:6085–6099. https://doi.org/10.1016/j.ijsolstr.2005.07.051
13. Zhandarov S, Mäder E (2005) Characterization of fiber/matrix interface strength: Applicability of different tests, approaches and parameters. Compos Sci Technol 65:149–160. https://doi.org/10.1016/j.compscitech.2004.07.003
14. Kelly A, Tyson WR (1965) Tensile properties of fibre-reinforced metals: Copper/tungsten and copper/molybdenum. J Mech Phys Solids 13:329–350. https://doi.org/10.1016/0022-5096(65)90035-9
15. Minnicino MA, Santare MH (2012) Modeling the progressive damage of the microdroplet test using contact surfaces with cohesive behavior. Compos Sci Technol 72:2024–2031. https://doi.org/10.1016/j.compscitech.2012.09.009
16. Yang L, Thomason JL, Zhu W (2011) The influence of thermo-oxidative degradation on the measured interface strength of glass fibre-polypropylene. Compos A Appl Sci Manuf 42:1293–1300. https://doi.org/10.1016/j.compositesa.2011.05.011
17. Yang L, Thomason JL (2012) Development and application of micromechanical techniques for characterising interfacial shear strength in fibre-thermoplastic composites. Polym Test 31:895–903. https://doi.org/10.1016/j.polymertesting.2012.07.001
18. Zhang L, Ren C, Zhou C et al (2015) Single fiber push-out characterization of interfacial mechanical properties in unidirectional CVI-C/SiC composites by the nano-indentation technique. Appl Surf Sci 357:1427–1433. https://doi.org/10.1016/j.apsusc.2015.10.018

19. Mueller WM, Moosburger-Will J, Sause MGR, Horn S (2013) Microscopic analysis of single-fiber push-out tests on ceramic matrix composites performed with Berkovich and flat-end indenter and evaluation of interfacial fracture toughness. J Eur Ceram Soc 33:441–451. https://doi.org/10.1016/j.jeurceramsoc.2012.09.009
20. Zidi M, Carpentier L, Chateauminois A, Sidoroff F (2000) Quantitative analysis of the micro-indentation behaviour of fibre-reinforced composites: Development and validation of an analytical model. Compos Sci Technol 60:429–437. https://doi.org/10.1016/s0266-3538(99)00143-8
21. Rodríguez M, Molina-aldareguía JM, González C, Llorca J (2012) A methodology to measure the interface shear strength by means of the fiber push-in test. Compos Sci Technol 72:1924–1932. doi: https://doi.org/10.1016/j.compscitech.2012.08.011
22. Molina-Aldareguía JM, Rodríguez M, González C, LLorca J (2010) An experimental and numerical study of the influence of local effects on the application of the fibre push-in test. Philos Mag 91:1293–1307. https://doi.org/10.1080/14786435.2010.480947
23. Medina C, Molina-Aldereguia J, Gonzales C et al (2015) Comparison of push-in and push-out test for measuring interfacial shear strength in nano-reinforced composite materials. J Compos Mater. https://doi.org/10.1177/0021998315595115
24. Mandell JF, Chen JH, McGarry FJ (1980) A microdebonding test for *in situ* assessment of fibre/matrix bond strength in composite materials. Int J Adhes Adhes 1:40–44. https://doi.org/10.1016/0143-7496(80)90033-0
25. Marshall DB, Oliver WC (1987) Measurement of interfacial mechanical properties in fiber-reinforced ceramic composites. J Am Ceram Soc 70:542–548. https://doi.org/10.2109/jcersj.100.530
26. Andrews EW, Garnich MR (2008) Stresses around fiber ends at free and embedded ply edges. Compos Sci Technol 68:3352–3357. https://doi.org/10.1016/j.compscitech.2008.09.001
27. Craven R, Pindoria S, Olsson R (2009) Finite element study of compressively loaded fibres fractured during impact. Compos Sci Technol 69:586–593. https://doi.org/10.1016/j.compscitech.2008.11.034
28. Buckley CP, Dooling PJ, Harding J, Ruiz C (2004) Deformation of thermosetting resins at impact rates of strain. Part 2: Constitutive model with rejuvenation. J Mech Phys Solids 52:2355–2377. https://doi.org/10.1016/j.jmps.2004.04.001
29. Xu Q, Tao W, Qu S, Yang Q (2015) A cohesive zone model for the elevated temperature interfacial debonding and frictional sliding behavior. Compos Sci Technol 110:45–52. https://doi.org/10.1016/j.compscitech.2015.01.018
30. Jäger J, Sause MGR, Burkert F et al (2015) Influence of plastic deformation on single-fiber push-out tests of carbon fiber reinforced epoxy resin. Compos A Appl Sci Manuf 71:157–167. https://doi.org/10.1016/j.compositesa.2015.01.011
31. Ojos DEL, Ghisleni R, Battisti A, et al (2016) Understanding the mechanical behavior of fiber / matrix interfaces during push-in tests by means of finite element simulations and a cohesive zone model. Comp Mater Sci 117:330–337. doi:https://doi.org/10.1016/j.commatsci.2016.02.009
32. Naya F, Gonz C (2016) Computational micromechanics of the transverse and shear behavior of unidirectional fiber reinforced polymers including environmental effects. Compos Part A. https://doi.org/10.1016/j.compositesa.2016.06.018
33. Pochiraju KV, Tandon GP, Schoeppner GA (2008) Evolution of stress and deformations in high-temperature polymer matrix composites during thermo-oxidative aging. Mech Time-Dependent Mater 12:45–68. https://doi.org/10.1007/s11043-007-9042-5
34. Welch BL (1947) The Generalization of Student's' Problem when Several Different Population Variances are Involved. Biometrika 34:28–35